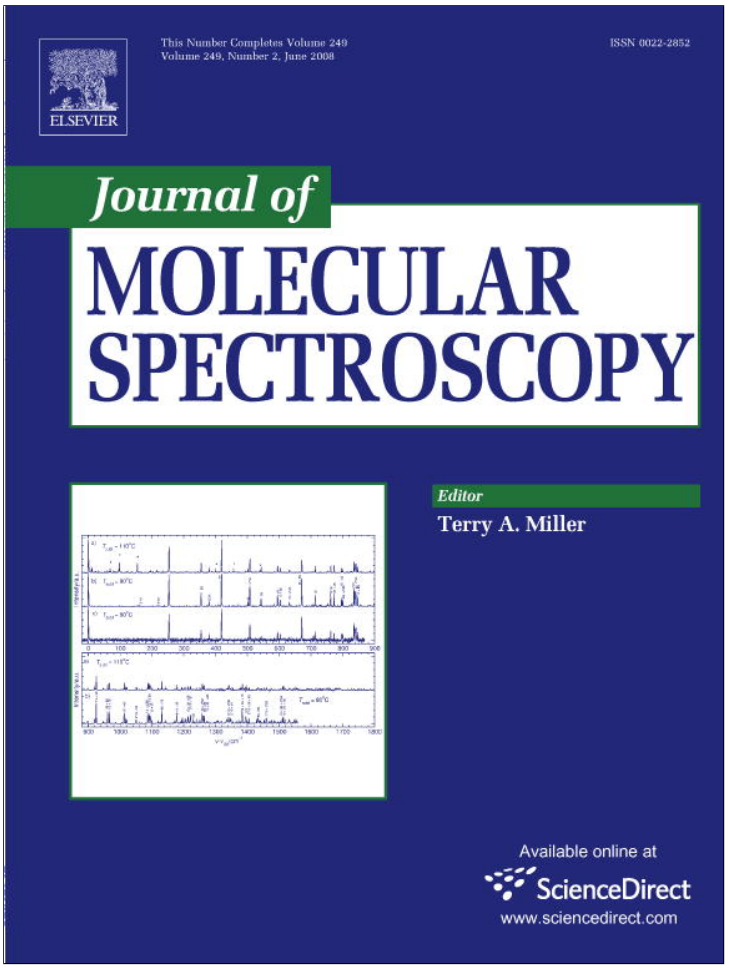

Journal of Molecular Spectroscopy 249 (2008) 86–94

Contents lists available at ScienceDirect

Journal of Molecular Spectroscopy

journal homepage: www.elsevier.com/locate/jms

Comparison between theoretical calculations and high-resolution measurements of pressure broadening for near-infrared water spectra

J.T. Hodges [a,*], D. Lisak [a,b], N. Lavrentieva [c], A. Bykov [c], L. Sinitsa [c], J. Tennyson [d], R.J. Barber [d], R.N. Tolchenov [d]

[a] Process Measurements Division, National Institute of Standards and Technology, 100 Bureau Drive, Gaithersburg, MD 20899, USA
[b] Instytut Fizyki, Uniwersytet Mikołaja Kopernika, ul. Grudziadzka 5/7, 87-100 Toruń, Poland
[c] Institute of Atmospheric Optics, av. Akademicheskii 1, Tomsk 634055, Russia
[d] Department of Physics & Astronomy, University College London, London WC1E 6BT, UK

ARTICLE INFO

Article history:
Received 31 January 2008
In revised form 26 February 2008
Available online 18 March 2008

Keywords:
Molecular spectroscopy
Water vapor
H2O
Cavity ring-down spectroscopy
Pressure broadening
Line shape

ABSTRACT

We report N_2 and air foreign pressure broadening coefficients of more than twenty rovibrational transitions of water vapor in the 935-nm spectral region, and these measurements are compared to new theoretical calculations. The data were obtained using the frequency-stabilized cavity ring-down spectroscopy method, yielding relative uncertainties for the broadening parameters in the range 0.4–2.2%. The sensitivity of measured broadening parameters to the choice of line shape functions is discussed, and systematic differences between experimentally determined collisional broadening coefficients are shown for the cases when the observed line narrowing is interpreted in terms of Dicke-narrowing or the speed-dependence of the collisional broadening and shifting. Theoretical models of pressure broadening for these transitions agree with the measurements to within 4% for most transitions with an average relative difference of 0.63%.

Published by Elsevier Inc.

1. Introduction

A quantitative understanding of molecular-transition line shapes is essential in many practical spectroscopic applications, including the remote sensing of gas temperature and pressure as well as retrievals of gas mixture composition. For such applications, databases of line parameters (assignments, intensities, width and shift parameters, etc.) exist for molecules contained in atmospheres of the Earth and other planets. See for example HITRAN 2004 [1] or others given in Refs. [2–4]. These databases are continuously improved to fulfill the increasingly demanding requirements of the newest remote sensing instruments, and line parameters with sub-1% accuracy are sometimes required [5]. This level of accuracy is often difficult to achieve in laboratory measurements because of complications associated with preparing samples of known concentration and uncertainties in spectroscopic measurements. Here we consider the spectroscopy of water, one of the most abundant and important molecules in the atmosphere. From an experimental perspective, the accurate measurement of water vapor's spectroscopic parameters (in particular the line intensity S) poses a unique challenge because H_2O has a tendency to stick to and desorb from bounding surfaces, making it difficult to prepare gas mixtures with known and stable concentrations. Moreover, as was shown before [6], the measurement of line intensities as well as collisional broadening coefficients at sub-1%-levels of accuracy may be achieved only by taking subtle line shape effects into account. The most important of the line shape effects are the collisional narrowing [7] and dependence of collisional broadening and shifting on molecular speed (the so-called speed-dependent effects) [8]. When these effects are sufficiently important, fitting the commonly used Voigt profile to experimental spectra causes systematic errors in the retrieval of line shape parameters. Such biases can affect measurement of S which is typically determined from the fitted spectral area.

The speed-dependent effects are particularly difficult to treat because for many molecular systems there is no simple analytical model that can adequately represent the speed-dependence of both pressure broadening and pressure shifting. In this case, line shapes of individual transitions must be modeled individually, making it difficult to incorporate speed-dependent effects into standardized spectral databases. Although theoretical calculations of pressure broadening parameters usually cannot achieve accuracies better than 1%, they can provide critical information on the speed-dependence of collisional parameters needed for analysis of the most precise experimental data and for predictions in situations where data is lacking.

* Corresponding author.
E-mail address: joseph.hodges@nist.gov (J.T. Hodges).

0022-2852/$ - see front matter Published by Elsevier Inc.
doi:10.1016/j.jms.2008.02.022

In the remainder of this paper we investigate collisional broadening parameters for H_2O broadened by N_2 and by air, and we specifically consider 21 transitions from the ground vibrational state to the $(v_1\,v_2\,v_3) = (2\,0\,1)$ vibrational band of H_2O occurring in the wave number region 10603–10732 cm^{-1}. We present line shapes measured at room temperature using the frequency-stabilized cavity ring-down spectroscopy (FS-CRDS) technique, and we report relative standard uncertainties less than 1%. We also discuss systematic effects associated with the dependence of the collisional broadening coefficient on the fitted line shape function. Finally, we present two sets of predictions for the observed line broadening and compare them to our measurements. Both sets of predictions used the corrected Anderson, Tsao, Curnutte (ATC) model of line broadening [9], the difference being that the H_2O energy levels and dipole transition moments were derived either from an effective Hamiltonian (EH) or a discrete variable representation (DVR) [10] for the nuclear motion. The EH approach is accurate when corrections arising from anharmonicity, Coriolis coupling or centrifugal distortion are small. This occurs when considering transitions to low-lying vibrational states for which the vibrational amplitudes are small in comparison with equilibrium distances between atoms, so that molecular properties such as multipole moments and polarizabilities can be accurately represented by a Taylor series expansion about equilibrium. In the case of transitions to highly-excited states, the Taylor series expansions are slowly convergent or even divergent because the vibrational motion cannot be considered to be of small amplitude, and consequently the DVR method gives more accurate wave functions than the EH method.

2. Experiment

2.1. Measurement technique

Water vapor line shapes were measured by the FS-CRDS method using a spectrometer built and operated at the National Institute of Standards and Technology (NIST). Detailed descriptions of this technique and the NIST FS-CRDS spectrometer can be found in Refs. [11,12]. The ring-down cavity consisted of two mirrors separated by about 73 cm and having high-reflectivity $R = 0.9997$ at the probe wavelength $\lambda_p = 931.9$–943.1 nm, and lower reflectivity $R = 0.97$ at the reference laser wavelength $\lambda_r = 633$ nm. The probe laser was a continuous wave external cavity diode laser (ECDL) having a Littrow cavity configuration and providing about 2 mW of power incident on the ring-down cavity. The reference laser was a frequency-stabilized HeNe laser (long-term stability of 1 MHz) that provided a stable optical frequency required for active control of the ring-down cavity mirror-to-mirror distance. Fluctuations in the HeNe laser were monitored by measuring the heterodyne beat note produced by interference of the reference laser and a separate I_2-stabilized HeNe laser having an absolute frequency stability of 10 kHz. Stabilization of the cavity length constrained the ring-down cavity resonant frequencies to a well-defined frequency comb of constant spacing which we used to calibrate the detuning axis of our spectral scans. The length-stabilization servo involved imposing a 20 kHz modulation (with a modulation depth of 2 MHz) on the HeNe frequency using a double-passed acousto-optic modulator (AOM), phase sensitive detection of the transmitted beam at the modulation frequency, and proportional and integral feedback of the error signal to the cavity length via a pzt-actuated mirror. The frequency stability of the comb of ring-down cavity modes was approximately 100 kHz using this stabilization scheme and was limited by our ability to compensate for the observed fluctuations in the HeNe laser frequency. By stepwise locking of the ECDL probe laser to successive longitudinal modes of the TEM_{00}, spectra of water vapor were probed by measuring the ring-down decay time constants $\tau(\nu)$ at each step. The intensity of light exiting the cavity was measured with a Si-PIN photoreceiver (10 MHz bandwidth) that was digitized by a 12-bit board mounted in a desktop computer. The absorption coefficient $\alpha(\nu)$ was calculated from $\alpha(\nu) + \alpha_{bg}(\nu) = 1/(c\tau)$, where $\alpha_{bg} \cong 4 \times 10^{-6}\ cm^{-1}$ corresponds to the baseline of spectrum and is associated with base losses of the ring-down cavity mirrors, c is the speed of light and ν is the radiation frequency. For a single isolated transition, the absorption coefficient is modeled by $\alpha(\nu) = n_a c\, S\, g(\nu - \nu_0)$, where the line shape function g is normalized to unity area $\int d\nu g(\nu - \nu_0) = 1$, and hence the line area $\mathcal{A} = \int d\nu \alpha(\nu) = n_a c S$. Here n_a denotes the absorber concentration, c is the speed of light and ν_0 is the transition frequency.

Note that the frequency difference between longitudinal modes is equal to the free-spectral-range (FSR) of the cavity (202.812(22) MHz). However, we were able to realize frequency steps much smaller than the FSR by precisely frequency shifting (50 kHz resolution see Ref. [13]) the reference HeNe laser with the AOM. We emphasize that since the ring-down cavity length was servoed to the frequency of the reference laser, this technique shifted the entire comb of resonant frequencies of the ring-down cavity in a controlled way. For the line shape measurements discussed in this article, we used steps in the range 50–100 MHz, which gave several 100 points per line profile. At each frequency step 300 ring-down signals were acquired, individual signals were fit using an exponential function and the fitted time constants were averaged. This method yielded measured spectra with signal-to-noise ratios of about 1000:1. Excellent linearity and low uncertainty for both the spectrum frequency and absorption axes of our spectrometer was demonstrated earlier [6,13,14], and using the FS-CRDS method to measure transitions of the O_2 A-band, we have recently demonstrated signal-to-noise ratios in excess of 6000:1 [15].

We carefully prepared and monitored the water vapor concentration in the ring-down cavity gas sampling system in order to optimize the quality of the experimental results. This effort was critical to the experiment because of well-known difficulties arising from persistent adsorption and desorption of water from bounding surfaces. We used a continuous flow of the gas mixture through the ring-down cell to mitigate these confounding effects. To further suppress these effects, all-metal seals and electro-polished stainless steel internal surfaces were used throughout the flow system and dead volumes were minimized. For generating the sample streams, purified N_2 carrier gas was metered through two mass flow controllers operated in parallel. The first stream (flow rate = 0.025 std. L min^{-1}) passed through the head-space of a temperature-regulated water-filled saturator, and the second stream (flow rate = 1.2 std. L min^{-1}) bypassed the saturator. Downstream of the saturator the two streams were recombined, and a portion (0.5 std. L min^{-1}) was diverted to a reference-grade chilled-mirror hygrometer (CMH) which measured the molar fraction of water vapor in the mixture. The combined stability of the saturator and CMH was approximately 0.4% in terms of water vapor molar fraction. The water vapor molar fraction ranged from about 10^{-4}–2.5×10^{-4} and was adjusted for each transition so that the peak absorption loss was approximately equal to the base loss of the ring-down cavity. The gas pressure, p, was measured with two NIST-calibrated capacitance diaphragm gauges having full scale responses of 13.3 kPa and a 133 kPa, respectively. Each pressure gauge had a relative combined standard uncertainty of 0.02%. The gas mixture passed through the ring-down cell with a constant flow rate of about 0.5 std. L min^{-1} and the total gas pressure in the ring-down cell was actively stabilized to within 0.1%. A calibrated 100-Ω platinum resistance thermometer (PRT) measured the exterior temperature, T, of the ring-down cell with a standard

uncertainty of 0.1 K. All measurements were made at room temperature and no effort was made to actively suppress small temperature variations. For all the spectra, the average measured temperatures were between $T = 297.7$ K and $T = 300.1$ K, and the temperature variation over the course of a given spectrum was typically less than 0.2 K. The measured broadening coefficients, $\gamma(T)$, reported below were corrected to a reference temperature of $T_r = 296$ K using the relation, $\gamma(T) = \gamma(T_r)(T_r/T)^n$, where n is the broadening half-width temperature exponent for each transition. Typically the temperature correction was less than 0.5% and was never greater than 1% of the measured value.

2.2. Line shape analysis

Table 1 contains the zero-pressure line positions, intensities, temperature exponents (for air broadening) and quantum assignments for the H_2O transitions investigated in this work. These data are taken from HITRAN 2004 [1]. For recent papers on water line shape studies see Refs. [16–19] and references therein.

In order to check for the influence of the collisional (Dicke) narrowing [7] and the speed-dependence of collisional parameters [8] on experimental line shapes, the Voigt profile (VP) was first fit to the data. The characteristic W-shaped residuals indicated the influence of line narrowing effects which, as mentioned by many authors, may be caused by Dicke-narrowing as well as by the speed-dependent effects. To investigate the influence of line shape models on fitted values of collisional broadening parameters the Galatry profile (GP) [20] was fitted as well as the speed-dependent Voigt profile (SDVP) [8]. The GP assumes a soft collision model, neglects the speed-dependent effects and assigns all the line narrowing to Dicke-narrowing. Opposite to the GP, the SDVP neglects Dicke-narrowing but takes the speed-dependent effects into account. Thus for the SDVP, line narrowing is interpreted as being caused only by the speed-dependent effects.

Fig. 1 (top panel) shows two representative experimental spectra and the respective GP fits for the 10603.52939 cm^{-1} H_2O line broadened by $p = 13.3$ kPa and $p = 26.7$ kPa of N_2, and fit residuals (bottom panel) for the $p = 26.7$ kPa condition corresponding to the VP, GP and SDVP cases. For the SDVP, the speed-dependence of collisional broadening and shifting was calculated using the DVR theory. The collisional broadening and shifting coefficients were calculated for different relative absorber–perturber speeds, varying between 0.05 and 4 times the most probable speed $v_{MP} = \sqrt{2k_BT/m_r}$. Here k_B is the Boltzmann constant, and m_r is the reduced mass of absorber–perturber system. For details of the SDVP calculation from such a temperature-dependence for the collisional parameters, see [21]. We also fitted the speed-dependent Voigt profile in which the speed-dependence was modeled by quadratic functions (see Ref. [22]). We denote the resulting line shape as the SDVPQ, and the residuals for this fit are also shown in the bottom panel of Fig. 1. We note that, compared to the VP and SDVP, the GP has one additional parameter, called the optical frequency of the velocity-changing collisions, ν_{opt}. This parameter is determined from the fits to experimental profiles. In contrast, the SDVPQ has two additional parameters (compared to the VP and SDVP) which describe the speed-dependence of collisional broadening and shifting determined from the best fits of the profile to experimental data.

The GP gives an excellent fit quality as can be seen by inspection of the fit residuals in Fig. 1. Only a slight asymmetry of the line, most probably due to speed-dependence of the pressure shift, remains because the GP is a symmetric profile. The SDVP with the calculated speed-dependence of collisional broadening and shifting gives a better fit quality than VP but it seems to overestimate the line narrowing effect. The SDVPQ with two adjustable parameters describing the speed-dependent effects gives flat residuals within the random noise. We also present (in the lowest panel of Fig. 1) residuals for the Voigt profile with variable Gaussian width (VP-G). This profile, also called the generalized Voigt profile [2,3] is sometimes used to take into account line narrowing effects. For example, it was used to analyze spectra published in ESA-WVB database [2,3]. As can be seen in Fig. 1 the VP-G gives relatively good residuals for our experimental data, but not as good as the GP or SDVPQ. The above analysis does not allow us to quantify the extent to which each of the two effects is responsible for narrowing of the lines investigated here. Most probably both Dicke-narrowing and the speed-dependent effects contribute significantly. However, we can quantify the systematic effect of the choice of line profile model on the fit-derived collisional broadening coefficients. In Fig. 2 the ratio γ_i/γ_{GP} is given as a function of N_2 pressure p_{N_2}. Here γ_i denotes the respective collisional widths determined from fits of the various profiles considered above, and γ_{GP} is the collisional width determined from fits of the GP. For this comparison we added values from fits of the Nelkin–Gha-

Table 1
$H_2{}^{16}O$ transition wave numbers $\tilde{\nu}_0$, intensities $S(T_r)$ and coefficients of temperature dependence for the air-broadened half-widths n

$\tilde{\nu}_0$ (cm^{-1})	$S(T_r)$ (10^{-22} cm^2 cm^{-1} molec.)	n	Q'	Q''	Branch	j_m	k_m
10687.36209	6.453	0.73	4 0 4	3 0 3	R	4	0
10667.76395	6.122	0.77	3 1 3	2 1 2	R	3	1
10603.52939	5.864	0.78	2 2 0	2 2 1	Q	2	2
10697.41667	5.203	0.69	5 1 5	4 1 4	R	5	1
10656.75002	5.200	0.78	2 0 2	1 0 1	R	2	0
10700.67209	4.755	0.73	4 1 3	3 1 2	R	4	1
10700.84183	1.642	0.69	5 3 3	4 3 2	R	5	3
10605.04424	4.396	0.78	1 1 1	1 1 0	Q	1	1
10605.18075	0.8485	0.77	3 2 1	3 2 2	Q	3	2
10660.71159	4.315	0.78	2 1 1	1 1 0	R	1	1
10711.08905	3.890	0.64	6 0 6	5 0 5	R	6	0
10698.94469	3.547	0.73	4 2 2	3 2 1	R	4	2
10704.42045	3.207	0.69	5 2 4	4 2 3	R	5	2
10670.12211	3.011	0.77	3 2 2	2 2 1	R	3	2
10673.52971	2.114	0.77	3 0 3	2 0 2	R	3	0
10683.38048	2.104	0.73	4 1 4	3 1 3	R	4	1
10683.69747	1.412	0.73	4 3 1	3 3 0	R	4	3
10730.42472	2.01	0.64	6 1 5	5 1 4	R	6	1
10730.22848	1.351	0.59	7 2 6	6 2 5	R	7	2
10731.01173	1.262	0.53	8 0 8	7 0 7	R	8	0
10731.39938	0.492	0.53	8 1 8	7 1 7	R	8	1

All lines correspond to the (201) ← (000) vibrational transition with the rotational assignment $Q = (J,K_a,K_c)$ (upper′: lower″). j_m and k_m are related to the rotational quantum numbers and are defined in the text. Quantities are from the HITRAN 2004 database [1].

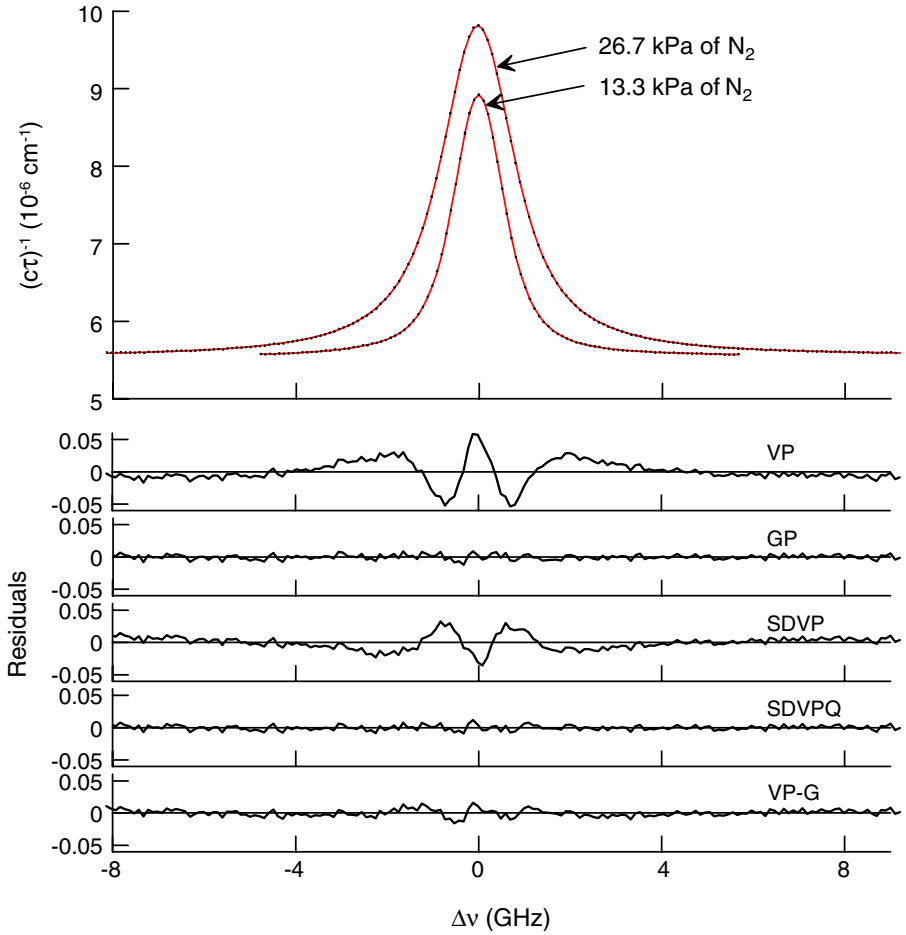

Fig. 1. Experimental absorption profiles of the 10603.52939 cm^{-1} H_2O line broadened by N_2 at 13.3 kPa and 26.7 kPa together with fitted Galatry profiles. Below are the residuals for p = 26.7 kPa, corresponding to the fits of different model line profiles: VP, GP, SDVP and SDVPQ. See in text for details.

tak profile (NGP [23,24] also called the Rautian profile) which, unlike the GP is based on the hard collision model, and which like the GP, takes Dicke-narrowing into account and neglects the speed-dependent effects. We note that the fit quality for the NGP was in most cases similar to the GP fits. As can be seen in Fig. 2 the three profiles having the best fit qualities (SDVPQ, GP, and NGP) give γ values that differ from each other by less than 3% with the GP-based value being in the middle. Taking this result into account we conclude that collisional broadening coefficients with sub-1% uncertainties must be interpreted together with the line shape model used for their determination. It is interesting that when the VP or VP-G is used, the collisional width γ not only differs by over 10% from the GP-, NGP- or SDVPQ-based values, but it also strongly depends on the pressure at which it was measured. For large pressure, where the Gaussian component of the VP is small compared to the Lorentzian part, this systematic effect is less important. We observed similar effects for H_2O lines in the 1.3 μm region [13]. Additionally, we note that the fitted ν_{opt} is

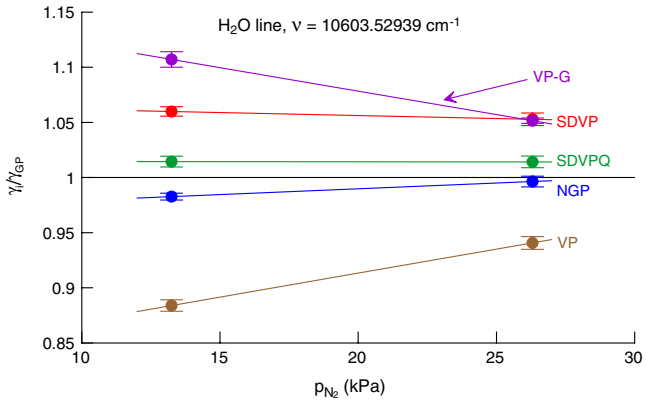

Fig. 2. Ratio of the pressure broadening coefficients γ_i obtained from the fits of different line shape models (VP, NGP, SDVP and SDVPQ) to γ_{GP} obtained from fits of GP model to experimental profiles of the 10603.52939 cm^{-1} H_2O line broadened by N_2 at p = 13.3 kPa and p = 26.7 kPa. Error bars correspond to standard uncertainties of these ratios.

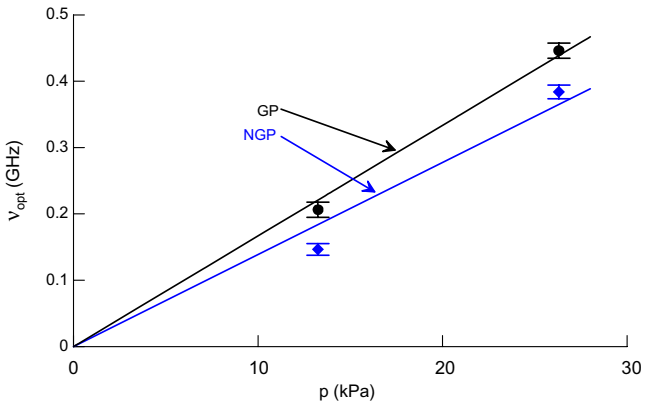

Fig. 3. Variation of the optical frequency of the velocity-changing collisions ν_{opt} with p, determined from GP and NGP fits. Results are for the 10603.52939 cm^{-1} line of H_2O broadened by N_2.

not linear with pressure when either the GP or the NGP are fitted to line profiles for which the speed-dependent effects play an important role. This effect was observed by many authors (e.g. [25–28]). To illustrate, we present in Fig. 3 a nonlinear pressure-dependence (over the range p = 13.3 kPa and 26.7 kPa) of ν_{opt} for foreign broadening by N_2 of the 10603.52939 cm^{-1} H_2O line.

3. Theoretical model for linewidth calculations

3.1. BT2 line list for water

A number of numerical procedures involving the direct solution of the Schrodinger equation [29–31] are available for calculating the rotation–vibration spectra of triatomic molecules such as water. Certain calculations of this type agree with measurements [32], and for water the accuracy of these calculations is determined by the quality of the available potential energy surface (PES) plus suitable allowance for failure of the Born–Oppenheimer approximation [33]. Several high-accuracy *ab initio* [33–35] and semi-empirical [34,36,37] potential energy surfaces are available for water. These calculations yield energy levels and associated nuclear motion wave functions. In ATC model described below we also require dipole transition moments which can be obtained using appropriate dipole moment surfaces (DMS). The best available DMS are the *ab initio* ones of Schwenke and Partridge [38] and Lodi et al. [39].

In this work we use energy levels and dipole transition moments from the BT2 line list [10]. This line list for water was constructed using the DVR3D nuclear motion suite [31] as the DVR of the H_2O nuclear motion. The BT2 line list also incorporated the semi-empirical (PES) of Shirin et al. [36] and the DMS of Schwenke and Partridge [38]. This line list, which includes transitions between rotation–vibration states of water up to 30 000 cm^{-1} above the ground state and rotational excitation with up to J = 50, comprises a total of 22 100 states and covers a much larger range than is required for the present study. This line list also gives dipole intensities for all rigorously allowed transitions without recourse to rules given by approximate quantum numbers. It contains a total of 5.08×10^8 transitions. Further information on the BT2 line list can be found in the original publication [10]. In addition to the DVR-based approach, energy levels and dipole transition moments were determined using an effective Hamiltonian (EH) based on standard perturbation methods.

3.2. Anderson, Tsao, Curnutte model

Here we use the ATC model [9], which is distinguished by its relative computational simplicity, to calculate from first principles the pressure broadening coefficients of H_2O broadened by N_2. It has proven to be efficient at describing line broadening processes for a number of molecules, such as HCl–DCl, H_2O–H_2O and H_2O–CO_2 which are characterized by so-called strong interactions, when the distance of closest approach, r_c, is less than the interruption parameter, b_0, of the Anderson theory.

For the case of weak interactions ($r_c > b_0$) the ATC method does not provide a good description. Therefore various cut-off-free methods for broadening calculations, which take into account increasingly fine effects such as atom–atom potentials, trajectory curvature and the imaginary part of the interruption function [40–43], have been proposed. These methods describe the processes rather well, but, because of the complexity of calculations, they do not allow for visualization or analysis of the processes occurring between the colliding molecules. This shortcoming is the main disadvantage of the ATC method and limits the extent to which the ATC can model pressure broadening effects arising from different scattering channels and pressure-induced shifts. It is therefore desirable to correct the ATC method [9] to eliminate this issue. To this end, some of us have proposed a semi-empirical version of such a correction [44] which is briefly described below.

According to the ATC theory the half-width γ_{if} associated with the $i \to f$ transition can be written as

$$\gamma_{if} = B(i,f) + \sum_l D^2(ii'|l) P_l^A(\omega_{ii'}) + \sum_l D^2(ff'|l) P_l^A(\omega_{ff'}) + \ldots, \tag{1}$$

where

$$B(i,f) = \frac{n}{c} \sum_k \rho(k) b_0^2(k,i,f) \tag{2}$$

is the averaged "interruption part" of the half-width, $D(ii'|l)$ and $D(ff',l)$ are the transition strengths (reduced matrix elements) associated with a multipole of rank l, and

$$P_l^A(\omega) = \frac{n}{c} \sum_k \rho(k) \sum_{l',k'} A_{ll'} D^2(kk'|l') F_{ll'} \left(\frac{2\pi c b_0(k,i,f)}{v} (\omega + \omega_{kk'}) \right) \tag{3}$$

is the efficiency function for the scattering channel $i \to i'$ or $f \to f'$ (if the appropriate frequencies $\omega_{ii'}$ and $\omega_{ff'}$ are substituted). In Eqs. (1)–(3) n is the number density of perturbing molecules, $\rho(k)$ is the thermal population of level k where k is the set of quantum numbers of the perturbing molecule, v is the average relative collision velocity and $F_{ll'}$ are the resonance functions. The terms $A_{ll'}$ correspond to ll'-type interactions. For example, in the case of the dipole–quadrupole interaction which has l = 1, l' = 2,

$$A_{12} = \frac{16q^2}{45h^2v^2b_0^6(k,i,f)}, \tag{4}$$

where h is Planck's constant and q is the quadrupole moment. The formulae are similar for the pressure shifting coefficients.

3.3. Correction to ATC theory

The sums in Eq. (3) include transitions of different tensor type (dipole, quadrupole and other) and can be represented as products of two different factors $D^2(ii'|l)$ and $P_l^A(\omega)$. The transition strengths $D^2(ii'|l)$ and $D^2(ff'|l)$ adapted to the scattering channels $i \to i', f \to f'$ depend only on the wave functions of the lower and upper states of the radiating molecule, and they can be regarded as well-known quantities which can be taken from calculations performed on the isolated molecule. However, the expansion coefficients in Eq. (1), $P_l(\omega_{ii'})$ and $P_l(\omega_{ff'})$ are influenced by intermolecular effects and can be regarded as the efficiency for a given scattering channel. They depend on the intermolecular potential, and the trajectory of relative motion, the energy levels and the multipole moments of the perturbing molecule. While the intramolecular factors $D(ii'|l)$ and $D(ff'|l)$ are often well-known, the intermolecular interaction parameters are usually determined with lower accuracy. It is useful to separate the terms in Eq. (1) into the well-known and only approximately known quantities, and to refine the latter by fits to the experimental data.

Our correction to the ATC involves defining a corrected form of $P_l^A(\omega)$ denoted by $P_{l,c}^A(\omega)$. As $P_l^A(\omega)$ is a smooth function of the angular frequency ω, it is consistent to represent its corrected value in the form

$$P_{l,c}(\omega) = C_l(\omega) P_l^A(\omega), \tag{5}$$

where $P_l^A(\omega)$ is the efficiency function of the Anderson theory and $C_l(\omega)$ is a correction factor, which is determined from fitting to experimental data. To realize the correction to the ATC, we substitute the corrected form, $P_{l,c}(\omega)$, for $P_l^A(\omega)$ in Eq. (1). Note that the function $P_l^A(\omega)$ remains the most important term in the calculation:

it determines all the main contributions to the broadening, whereas the factor $C_l(\omega)$ gives only a small correction. For the present calculations we have used the correction factor and fitting parameters from [44].

Calculations of line contour parameters and their temperature exponents have been made using this method for numerous cases including the H_2O–N_2 [45–48], CO_2–N_2 and CO_2–O_2 collision systems [44]. The results of these calculations have been included in the freely available carbon dioxide spectroscopic data bank [49] and in the "ATMOS" Informational System [50].

4. Comparison of measured and predicted linewidths

In Table 2 the experimental values of N_2 broadening coefficients γ_{CRDS} derived from the GP fits are given with their standard uncertainties. For eight of these transitions, we also present the N_2 broadening data of Giver et al. [51] denoted by γ_{Giver}. They measured N_2 broadening of water vapor using a multipass cell and grating spectrometer with a wave number resolution of 0.046 cm^{-1} and fit their measured spectra with Voigt profiles to determine the broadening coefficients. Comparing their measurements to the present results suggests a systematic discrepancy, the Giver data being about 3.1% greater than the CRDS-data on the average. We also present theoretical values, γ_{DVR} and γ_{EH}, calculated using the two methods mentioned in Section 1. For completeness and to enable reproduction of our experimental data using the Galatry profile, the fit-derived collisional narrowing coefficients $\beta = \nu_{opt}/p$ are also reported. Here p denotes the perturbing gas pressure. We note that, because of the nonlinear dependence of ν_{opt} on p, GP simulations that use the β values reported in Table 2 and that correspond to pressures higher than those presented in this paper may lead to systematic distortion of line shapes.

Using the empirical approach given by Brown et al. [52] for correlating water vapor air broadening and shifting coefficients as a function of vibrational and rotational quanta, we plot γ_{CRDS} against the quantity $k_m + 0.1 \times j_m$ in Fig. 4. The k_m and j_m terms for each transition are given in Table 1 and are defined in terms of the upper- and lower-state rotational quantum numbers (J,K_a,K_c). By definition, $j_m = J''$ for P- and Q-branch transitions and $j_m = J'$ for R-branch transitions. Likewise, $k_m = K_a''$ for $\Delta K_a = 0$ or $\Delta K_a = -1$ and $k_m = K_a'$ for $\Delta K_a = 1$. The factor of 0.1 in the abscissa coordinates is arbitrarily chosen to separate the data pairs in the horizontal direction. This approach effectively clusters the results into subsets having a fixed value of k_m in order to reveal systematic correlation with rotational quantum numbers. For comparison, the temperature-corrected data of Giver [51] are also shown. Inspection of Fig. 4 shows that γ tends to rapidly decrease with increasing j_m at fixed k_m, and as k_m increases there is a slower decrease in γ at fixed j_m. For $k_m = 0$, the change in γ appears to vary monotonically with j_m, whereas the variation in γ with j_m exhibits more complicated behavior for all other k_m. These results are in qualitative agreement with those of Brown et al., who evaluated these types of correlations for their air broadening data. They considered all of the transitions of the present study as well as 100s of others corresponding to seven overtone and combination vibrational bands of $H_2{}^{16}O$ with transition frequencies in this spectral region.

To compare theoretical and experimental results we evaluated the relative differences between the theoretical and experimental collisional broadening coefficients, and the results are summarized in Fig. 5. As in Fig. 4, we use the quantity $k_m + 0.1 \times j_m$ for the abscissa in panel A of Fig. 5. For the experimental results, relative standard uncertainties $u_r(\gamma_{CRDS})$ are given by the bracketed data points centered about zero. In most cases $u_r(\gamma_{CRDS})$ is less than 1%. For most lines, the relative differences between theoretical and experimental values of γ are smaller than 4%, whereas in the extreme case it is 11%. The differences between the theoretical and measured values correlate with k_m and j_m, and in particular for the DVR and EH-based calculations the best and worst agreement occurs for $k_m = 0$, and $k_m = 2$, respectively. However, no systematic dependence in the relative differences was found with line intensity. The average relative difference (for all transitions considered here) between the theoretical and experimental profiles, defined as $(\gamma_{theor} - \gamma_{CRDS})/\gamma_{CRDS}$, is −0.63% for DVR results and −0.97% for the EH results. This difference is small compared to the disagreements for individual lines. The absolute value of the relative difference $|(\gamma_{theor} - \gamma_{CRDS})/\gamma_{CRDS}|$ averaged over all transitions (this number characterizes the scatter in the results) is 1.7% for the DVR and 2.9% for the EH. Also comparison of the

Table 2
Experimental, γ_{CRDS} and γ_{Giver}, and theoretical, γ_{DVR} and γ_{EH}, pressure broadening coefficients (HWHM) of H_2O lines broadened by N_2 at $T_r = 296$ K

$\tilde{\nu}_0$ (cm^{-1})	γ_{CRDS}	γ_{Giver}	β	γ_{DVR}	γ_{EH}
10687.36209	0.03096(13)	0.0320(10)	0.0157(15)	0.0317	0.0320
10667.76395	0.03202(19)		0.0185(27)	0.0317	0.0320
10603.52939	0.03091(14)	0.0319(3)	0.0170(19)	0.0309	0.0299
10697.41667	0.02826(21)	0.0299(4)	0.0148(12)	0.0287	0.0287
10656.75002	0.03381(20)		0.0222(41)	0.0334	0.0343
10700.67209	0.03176(20)	0.0330(6)	0.0203(29)	0.0323	0.0317
10700.84183	0.02731(56)		0.0141(1)	0.0260	0.0251
10605.04424	0.03411(15)		0.0222(36)	0.0331	0.0331
10605.18075	0.03056(65)		0.0121(59)	0.0308	0.0302
10660.71159	0.03372(23)		0.0228(33)	0.0334	0.0334
10711.08905	0.02557(24)	0.0260(3)	0.0120(6)	0.0257	0.0263
10698.94469	0.03058(12)		0.0169(12)	0.0308	0.0305
10704.42045	0.02840(41)		0.0144(19)	0.0284	0.0275
10670.12211	0.03087(15)	0.0307(3)	0.0164(14)	0.0302	0.0296
10673.52971	0.03274(17)		0.0209(20)	0.0327	0.0334
10683.38048	0.03063(22)	0.0318(10)	0.0166(12)	0.0308	0.0311
10683.69747	0.02836(23)	0.0293(4)	0.0147(12)	0.0263	0.0251
10730.42472	0.02937(24)		0.0174(14)	0.0302	0.0296
10730.22848	0.02492(22)		0.0157(17)	0.0243	0.0237
10731.01173	0.01920(33)		0.0119(4)	0.0189	0.0195
10731.39938	0.01856(18)		0.0121(17)	0.0186	0.0195

The CRDS-based coefficients are based on Galatry fits, and those of Giver et al. [51] were based on Voigt profiles and were converted from STP conditions using a temperature exponent $n = 0.62$. The CRDS-measured collisional narrowing coefficients are given by β. All γ and β coefficients are in units of (MHz Pa^{-1}). To convert γ and β coefficients to the more commonly used units of (cm^{-1} atm^{-1}), multiply the tabulated values by 3.3798382 (cm^{-1} atm^{-1})/(MHz Pa^{-1}).

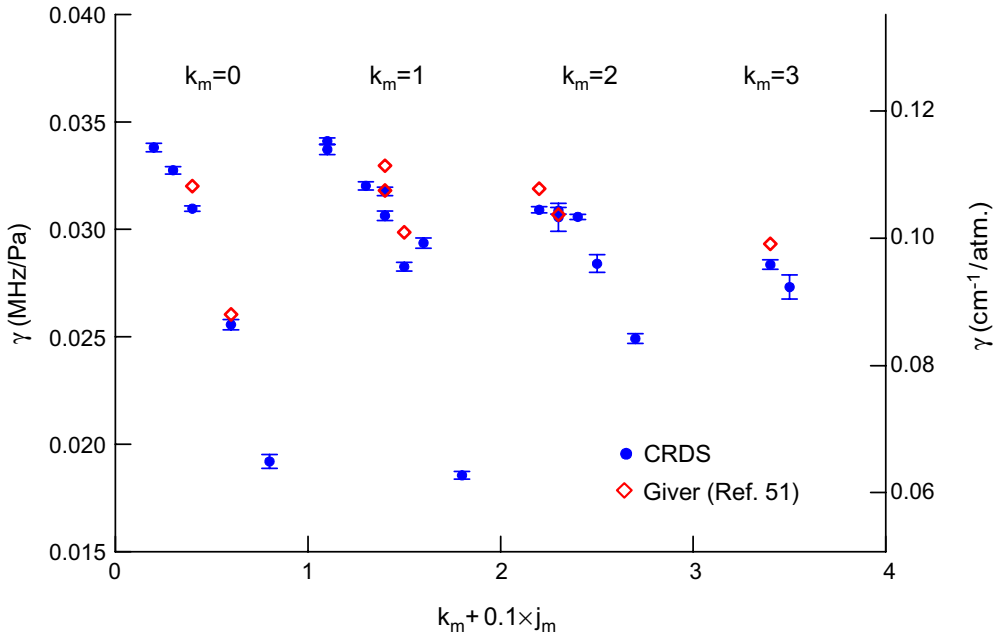

Fig. 4. CRDS-measured broadening coefficients for H_2O transitions for broadening by N_2. Values based on Galatry fits. Previously published data of Giver et al. [51], corrected to T_r = 296 K, are also shown.

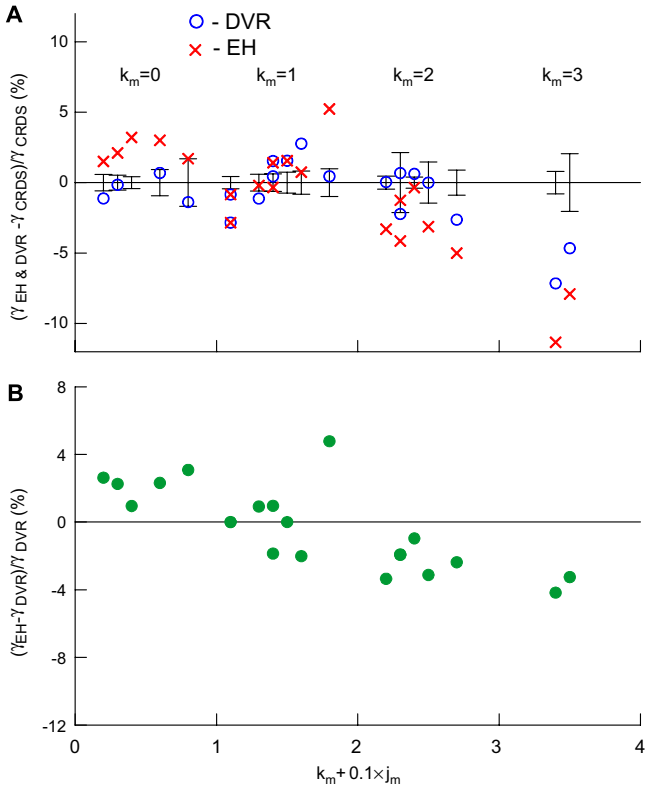

Fig. 5. (A) Relative differences between experimental and theoretical values of N_2-induced broadening coefficients of H_2O lines. Error bars indicate standard uncertainties of experimental results. (B) Relative differences between results from two theoretical methods: DVR and EH.

two theoretical methods, shown in Fig. 5B, suggests an increasing discrepancy as k_m increases. Nevertheless, in most cases the two sets of predictions differ from each other by less than 4%: an amount which is comparable to the disagreement between the theoretical and experimental results. As it was shown in [45] the half-widths calculated using variational wave functions disagree with those obtained using the standard approach of perturbative wave functions from Watson's effective Hamiltonian starting from 10 000 cm^{-1}. The difference between values obtained by the two methods is small in the present spectral region but grows with vibrational excitation and may achieve 10% at about 13 000 cm^{-1}.

For some of the H_2O lines considered here, we also measured their line shapes broadened by air. To this end, we used synthetic hydrocarbon-free air having a molar fraction of 0.795(5)% for N_2 and 0.205(5)% for O_2 in order to compare the pressure broadening coefficients with existing databases. In Table 3 our experimental values of the air-induced collisional broadening coefficients γ, determined from the GP fits, are compared to values reported in HITRAN 2004 [1], γ_{HT}, and in the ESA-WVB [2,3], γ_{ESA}, databases as well as with our theoretical results, γ_{DVR}. Note that the HITRAN 2004 values for these coefficients come from Brown et al. [52]. For completeness, we also note that an update to the HITRAN 2004 water line list was released in 2006. However for the transitions considered here, the differences between the updated and HITRAN 2004 values of the air-induced collisional broadening coefficients are negligible. Theoretical collisional broadening coefficients for O_2 broadening, denoted by $\gamma_{DVR}^{O_2}$ and used to calculate the γ_{DVR}, and experimental collisional narrowing coefficients β are also given in Table 3. In Fig. 6 we present a comparison similar to that given in Fig. 5A. As can be seen all the HITRAN 2004 values, and all except one ESA-WVB value agree with our experimental coefficients to within their combined standard uncertainties. Here we note that γ given in HITRAN 2004 as well as in ESA-WVB were determined from fits of the Voigt profile (with variable Gaussian width for ESA-WVB) and generally should differ systematically from our results based on GP fits. However, as shown in Fig. 2 these differences decrease for increasing pressure and near atmospheric pressures this systematic effect should be much smaller than uncertainties for individual lines in both databases presented

Table 3
Experimental γ_{CRDS}, and theoretical γ_{DVR} pressure broadening coefficients (HWHM) of H_2O lines broadened by hydrocarbon-free synthetic air at T_r = 296 K

ν_0 (cm^{-1})	γ_{CRDS}	β	γ_{DVR}	$\gamma_{DVR}^{O_2}$	γ_{HT}	γ_{ESA}
10687.36209	0.02849(17)	0.0149(10)	0.0283	0.0150	0.0285	0.0280
10667.76395	0.02891(20)	0.0135(13)	0.0284	0.0152	0.0289	0.0291
10603.52939	0.02800(12)	0.0132(5)	0.0269	0.0143	0.0283	0.0278
10697.41667	0.02532(8)	0.0124(3)	0.0257	0.0130	0.0254	0.0255
10656.75002	0.03133(44)	0.0208(13)	0.0309	0.0163	0.0030	0.0302
10711.08905	0.02377(17)	0.0132(8)			0.0229	0.0228

These measurements are compared to values reported in HITRAN 2004 [1] γ_{HT} and ESA-WVB [2,3] γ_{ESA} databases. The manufacturer's-specified molar-based composition was 0.795(5) for N_2 and 0.205(5) for O_2. This 0.5% uncertainty in composition introduces a systematic relative uncertainty of 0.25% in the collisional broadening coefficients. The uncertainties specified below include only those due to the fitting procedure. The O_2 broadening coefficients $\gamma_{DVR}^{O_2}$ used to calculate γ_{DVR} for air are also given. The experimental coefficients are based on the GP fits, also experimental collisional narrowing coefficients β are reported. All γ and β coefficients are in units of (MHz Pa^{-1}). To convert γ and β coefficients to the more commonly used units of (cm^{-1} atm^{-1}), multiply the tabulated values by 3.3798382 (cm^{-1} atm^{-1})/(MHz Pa^{-1}).

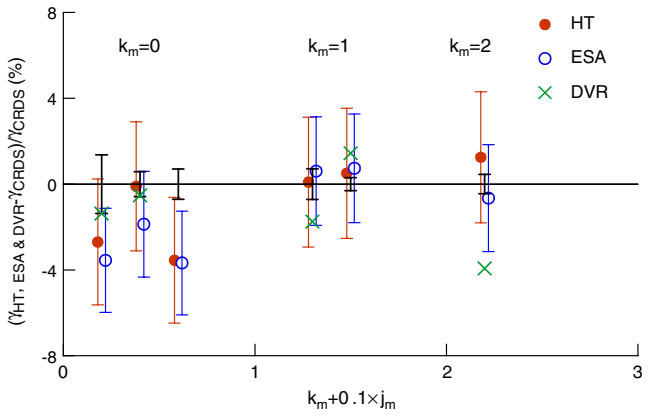

Fig. 6. Relative differences between air-induced broadening coefficients of H_2O lines and those measured in this work. HT and ESA values are from the HITRAN 2004 [1] and ESA [2,3] spectral databases, respectively.

in Fig. 6. Our theoretical values calculated here agree with experimental results to within 4%. This result suggests that our theoretical calculations generate collisional broadening coefficients that are as good as previously published data for the transitions considered here.

5. Conclusions

We measured foreign pressure broadening by N_2 of more than twenty relatively strong H_2O transitions in the 930–940 nm spectral region. Of the transitions within this set, we also investigated six that were broadened by air. In most cases, we demonstrated a relative standard uncertainty smaller than 1% for the collisional broadening coefficient. The influence of line shape model on the measured collisional broadening coefficients was discussed. We also presented theoretical calculations of collisional broadening coefficients and compared these to the measured values. The agreement between experimental and theoretical coefficients was in most cases better than 4% and exhibited no systematic shift. Our air broadening coefficients agree with values from existing databases to their combined standard uncertainties, although we note that our relative uncertainties are significantly smaller than those of these previous measurements. The theoretical calculations presented here give values of collisional broadening coefficients as good as the experimental coefficients from the HITRAN 2004 and ESA-WVB databases, however, coefficients for more lines should be compared to draw such a general conclusion.

Our calculated speed-dependencies of the pressure broadening and shifting coefficients overestimate the observed line narrowing effect. This complication prevented us from using more advanced line shape models (without introducing additional empirical fit parameters) that simultaneously take into account both the speed-dependent effects and collisional narrowing, like for example the speed-dependent Nelkin–Ghatak profile (SDNGP) [24,53,54] or the speed-dependent billiard-ball profile (SDBBP) [55,56]. It is likely that one must use profiles that incorporate both Dicke-narrowing and the speed-dependent effects in order to obtain a linear dependence of the collisional narrowing parameter with pressure over a wide pressure range. Moreover, additional subtle line shape effects that cause line asymmetry, such as correlations between velocity-changing and dephasing collisions [57–59] or line mixing [60,61] could be investigated and quantified if the contribution of the speed-dependence of collisional parameters to the line shape formation were precisely known for the transitions investigated here.

Acknowledgments

The authors thank the NIST Office of Microelectronics Programs for supporting this work. This project was also supported by a Royal Society Joint Project grant and has been performed as part of IUPAC Task Group 2004-035-1-100 on "A database of water transitions from experiment and theory".

References

[1] L.S. Rothman, D. Jacquemart, A. Barbe, D.C. Benner, M. Birk, L.R. Brown, M.R. Carleer, K. Chance, L.H. Coudert, V. Dana, V.M. Devi, J.-M. Flaud, R.R. Gamache, A. Goldman, J.-M. Hartmann, K.W. Jucks, A.G. Maki, J.-Y. Mandin, S.T. Massie, J. Orphal, A. Perrin, C.P. Rinsland, M.A.H. Smith, J. Tennyson, R.N. Tolchenov, R.A. Toth, J.V. Auwera, P. Varanasi, G. Wagner, Radiat. Trans. 96 (2004) 139.
[2] R. Schermaul, R.C.M. Learner, D.A. Newnham, R.G. Williams, J. Ballard, N.F. Zobov, D. Belmiloud, J. Tennyson, J. Mol. Spectrosc. 208 (2001) 32.
[3] R. Schermaul, R.C.M. Learner, D.A. Newnham, J. Ballard, N.F. Zobov, D. Belmiloud, J. Tennyson, J. Mol. Spectrosc. 208 (2001) 43.
[4] M.F. Mérienne, A. Jenouvrier, C. Hermans, A.C. Vandaele, M. Carleer, C. Clerbaux, P.-F. Coheur, R. Colin, S. Fally, M. Bach, Radiat. Trans. 82 (2003) 99.
[5] C.E. Miller, L.R. Brown, R.A. Toth, D.C. Benner, V. Malathy Devi, CR Phys. 6 (2005) 876.
[6] D. Lisak, J.T. Hodges, R. Ciuryło, Phys. Rev. A 73 (2006) 012507.
[7] R.H. Dicke, Phys. Rev. 89 (1953) 472.
[8] P.R. Berman, J. Quant. Spectrosc. Radiat. Trans. 12 (1972) 1331.
[9] C.J. Tsao, B. Curnutte, J. Quant. Spectrosc. Radiat. Trans. 2 (1961) 41.
[10] R.J. Barber, J. Tennyson, G.J. Harris, R.N. Tolchenov, Mon. Not. R. Astron. Soc. 368 (2006) 1087.
[11] J.T. Hodges, H.P. Layer, W.W. Miller, G.E. Scace, Rev. Sci. Instrum. 75 (2004) 849.
[12] J.T. Hodges, R. Ciuryło, Rev. Sci. Instrum. 76 (2005) 023112.
[13] D. Lisak, J.T. Hodges, Appl. Phys. B 88 (2007) 317.
[14] J.T. Hodges, D. Lisak, Appl. Phys. B 85 (2006) 375.
[15] D.J. Robichaud, J.T. Hodges, D. Lisak, C.E. Miller, M. Okumura, J. Quant. Spectrosc. Radiat. Trans. 109 (2008) 435.
[16] M. Lepère, A. Henry, A. Valentin, C. Camy-Peyret, J. Mol. Spectrosc. 208 (2001) 25.
[17] R.A. Toth, J. Quant. Spectrosc. Radiat. Trans. 9 (2005) 1.
[18] R.A. Toth, J. Quant. Spectrosc. Radiat. Trans. 94 (2005) 51.

[19] H. Tran, D. Bermejo, J.L. Domenech, P. Joubert, R.R. Gamache, J.M. Hartmann, J. Quant. Spectrosc. Radiat. Trans. 108 (2007) 126.
[20] L. Galatry, Phys. Rev. 122 (1961) 1218.
[21] R. Ciuryło, A. Bielski, S. Brym, J. Jurkowski, J. Quant. Spectrosc. Radiat. Trans. 53 (1995) 493.
[22] D. Priem, F. Rohart, J.M. Colmont, G. Wlodarczyk, J.P. Bouanich, J. Mol. Struct. 517 (2000) 435.
[23] M. Nelkin, A. Ghatak, Phys. Rev. 135 (1964) A4.
[24] S.G. Rautian, I.I. Sobelman, Usp. Fiz. Nauk. 90 (1966) 209; S.G. Rautian, I.I. Sobelman, Sov. Phys. Usp. 9 (1967) 701.
[25] P. Duggan, P.M. Sinclair, A.D. May, J.R. Drummond, Phys. Rev. A 51 (1995) 218.
[26] J.F. D'Eu, B. Lemoine, F. Rohart, J. Mol. Spectrosc. 212 (2002) 96.
[27] D. Lisak, G. Rusciano, A. Sasso, J. Mol. Spectrosc. 277 (2004) 162.
[28] D. Lisak, G. Rusciano, A. Sasso, Phys. Rev. A 72 (2005) 012503.
[29] J. Tennyson, S. Miller, Comput. Phys. Commun. 55 (1989) 149.
[30] D.W. Schwenke, J. Phys. Chem. 100 (1996) 2867.
[31] J. Tennyson, M.A. Kostin, P. Barletta, G.J. Harris, J. Ramanlal, O.L. Polyansky, N.F. Zobov, Comput. Phys. Commun. 163 (2004) 85.
[32] O.L. Polyansky, J. Tennyson, J. Chem. Phys. 110 (1999) 5056.
[33] O.L. Polyansky, A.G. Csaszar, S.V. Shirin, N.F. Zobov, P. Barletta, J. Tennyson, D.W. Schwenke, P.J. Knowles, Science 299 (2003) 539.
[34] H. Partridge, D.W. Schwenke, J. Chem. Phys. 106 (1997) 4618.
[35] P. Barletta, S.V. Shirin, N.F. Zobov, O.L. Polyansky, J. Tennyson, E.F. Valeev, A.G. Csaszar, J. Chem. Phys. 125 (2006) 204307.
[36] S.V. Shirin, O.L. Polyansky, N.F. Zobov, P. Barletta, J. Tennyson, J. Chem. Phys. 118 (2003) 2124.
[37] S.V. Shirin, O.L. Polyansky, N.F. Zobov, R.I. Ovsyannikov, A.G. Csaszar, J. Tennyson, J. Mol. Spectrosc. 236 (2006) 216.
[38] D.W. Schwenke, H. Partridge, J. Chem. Phys. 113 (2000) 6592.
[39] L. Lodi, R.N. Tolchenov, J. Tennyson, A.E. Lynas-Gray, S.V. Shirin, N.F. Zobov, O.L. Polyansky, A.G. Csaszar, J. van Stralen, L. Visscher, J. Chem. Phys. 128 (2008) 044304.
[40] D. Robert, J. Bonamy, J. Phys. 40 (1979) 923.
[41] R. Lynch, R. Gamache, S.P. Neshyba, J. Chem. Phys. 105 (1996) 5711.
[42] A.D. Bykov, N.N. Lavrent'eva, L.N. Sinitsa, Atmos. Oceanic Opt. 5 (1992) 587.
[43] J. Buldyreva, J.J. Bonamy, D. Robert, J. Quant. Spectrosc. Radiat. Trans. 62 (1999) 321.
[44] S.A. Tashkun, V.I. Perevalov, J.-L. Teffo, A.D. Bykov, N.N. Lavrent'eva, J. Quant. Spectrosc. Radiat. Trans. 82 (2003) 165.
[45] A.D. Bykov, N.N. Lavrentieva, T.P. Mishina, L.N. Sinitsa, R.J. Barber, R.N. Tolchenov, J. Tennyson, J. Quant. Spectrosc. Radiat. Trans., in press., doi:10.1016/j.jqsrt.2008.01.006.
[46] C. Camy-Peyret, A. Valentin, Ch. Claveau, A. Bykov, N. Lavrentieva, V. Saveliev, L. Sinitsa, J. Mol. Spectrosc. 224 (2004) 164.
[47] V. Zeninari, B. Parvitte, D. Courtois, N.N. Lavrentieva, Yu.N. Ponomarev, G. Durry, Mol. Phys. 102 (2004) 1697.
[48] N.N. Lavrent'eva, Opt. Spektrosk. 96 (2004) 247.
[49] <ftp://ftp.iao.ru/pub/CDSD-1000>.
[50] <http://saga.atmos.iao.ru>.
[51] L.P. Giver, B. Gentry, G. Schwemmer, T.D. Wilkerson, J. Quant. Spectrosc. Radiat. Trans. 27 (1982) 423.
[52] L.R. Brown, R.A. Toth, M. Dulick, J. Mol. Spectrosc. 212 (2002) 57.
[53] D. Robert, J.M. Thuet, J. Bonamy, S. Temkin, Phys. Rev. A 47 (1993) R771.
[54] B. Lance, G. Blanquet, J. Walrand, J.-P. Bouanich, J. Mol. Spectrosc. 185 (1997) 262.
[55] R. Blackmore, J. Chem. Phys. 87 (1987) 791.
[56] R. Ciuryło, D.A. Shapiro, J.R. Drummond, A.D. May, Phys. Rev. A 65 (2002) 012502.
[57] A.S. Pine, J. Chem. Phys. 101 (1994) 3444.
[58] A.S. Pine, J. Quant. Spectrosc. Radiat. Trans. 62 (1999) 397.
[59] R. Wehr, A. Vitcu, R. Ciuryło, F. Thibault, J.R. Drummond, A.D. May, Phys. Rev. A 66 (2002) 062502.
[60] A.S. Pine, J. Quant. Spectrosc. Radiat. Trans. 57 (1997) 145.
[61] G.D. Sheldon, P.M. Sinclair, M.P. Le Flohic, J.R. Drummond, A.D. May, J. Mol. Spectrosc. 192 (1998) 406.